Small diameter electrospun silk fibroin vascular grafts: Mechanical properties, *in vitro* biodegradability, and *in vivo* biocompatibility

Valentina Catto [a,b], Silvia Farè [a,b,*], Irene Cattaneo [c], Marina Figliuzzi [c], Antonio Alessandrino [d], Giuliano Freddi [d], Andrea Remuzzi [c,e], Maria Cristina Tanzi [a,b]

[a] *Biomaterials Laboratory, Department of Chemistry, Materials and Chemical Engineering "G. Natta", Politecnico di Milano, Piazza L. Da Vinci 32, Milano, Italy*
[b] *Local Unit Politecnico di Milano, INSTM, Italy*
[c] *IRCCS — Istituto di Ricerche Farmacologiche Mario Negri, Bioengineering Department, via Stezzano 87, Bergamo, Italy*
[d] *INNOVHUB — SSI, Div. Stazione Sperimentale per la Seta, via G. Colombo 83, Milan, Italy*
[e] *Università di Bergamo, Industrial Engineering Department, Via Marconi 5, Dalmine, Bergamo, Italy*

1. Introduction

Due to the increase of both peripheral arterial occlusive diseases and coronary heart diseases, every year there is a strong patient demand for small diameter vascular grafts (internal diameter (*ID*) < 6 mm). Al-though synthetic polymeric materials (*i.e.* Dacron®, Goretex®) have been successfully used for large and medium diameter vessels (*ID* ≥ 6 mm), they fail at smaller diameters (*ID* < 6 mm), due to throm-bosis, anastomotic intimal hyperplasia, aneurysm formation, infection, and compliance mismatches [1–3]. To date, autologous vessels (*e.g.* sa-phenous vein or internal mammary artery) remain the clinical gold standard for small diameter vessel replacement, despite their scarce availability [1–3]. For these reasons, vascular tissue engineering repre-sents a possible innovative approach, developing functional alternative solutions.

* Corresponding author at: Biomaterials Laboratory, Department of Chemistry, Materials and Chemical Engineering "G. Natta", Politecnico di Milano, P.zza L. da Vinci 32, 20133 Milano, Italy.
E-mail address: silvia.fare@polimi.it (S. Farè).

The design requirements of an ideal small diameter vascular graft are stringent and mainly regard biocompatibility and appropriate mechanical properties. Specifically, tissue engineered vascular grafts should be non-toxic, biocompatible and non-thrombogenic [3–5]. Fur-thermore they should be able to support the variation in blood pressure and the blood flow without outflows, due to appropriate structure and suitable mechanical properties in terms of compliance, burst pressure, strength and suture retention [3–5]. After *in situ* implantation, tissue engineered vascular grafts should remodel into a functional blood ves-sel, in particular they should promote the complete regeneration of the endothelium [3–5]. Tissue engineered vascular grafts have been de-veloped using decellularized matrices (such as porcine abdominal aorta and carotid [6], human umbilical artery [7]), biodegradable synthetic polymers (such as polyglycerol sebacate (PGS) [8], poly-ε-caprolactone (PCL) [9,10]) or natural polymers (such as recombinant human tropoelastin [11], fibrin [12], silk fibroin [5]) [3,4]. To attract cells into the vessel graft, natural polymers are studied and used for the scaffold fabrication due to their similarity with human tissues. Among them, silk fibroin appears very promising for its peculiar properties. Silks are spun into fibers by some lepidopters or spiders and, depending on the

source, have specific composition, structure and properties [13]. Silk from the silkworm *Bombyx mori* is the most extensively used and characterized for biomedical application [13]. *Bombyx mori* silk fibers are composed of two filaments of the protein fibroin, coated by a glue-like protein, sericin [13–15]. The sericin was identified as a possible source of non physiological inflammatory reaction, and therefore usually removed by a degumming process [13–15]. After degumming silk fibroin (SF) presents high biocompatibility, excellent mechanical properties, and versatile processability. Consequently, SF has emerged as an attractive biomaterial for producing scaffolds for several applications in tissue engineering [13,15].

One of the key elements of tissue engineering is typically the produc-tion of ideal scaffolds able to mimic the native structure of the extracel-lular matrix (ECM), promoting the repopulation of the scaffold by host cells and the production of a new natural ECM. Following a biomimetic approach, nanofibrous scaffolds (made of fibers with diameters be-tween 1 and 1000 nm) are widely used for tissue engineering applica-tions due to the similarity with the size of native ECM fibers [16–18]. The most common methods used for nanofiber production are self-assembly, phase separation and electrospinning [1,16]. Among these techniques, electrospinning (ES) is the simplest and the most efficient process; in addition, it is a versatile method that is able to produce con-tinuous fibers, ranging from few nanometers to some micrometers, using several materials (polymers, blends of polymers, polymers loaded with other materials or additives such as inorganic particles, growth fac-tors, other biomolecules and living cells [17]) [4,16–18]. Furthermore, electrospun scaffolds are characterized by a high surface to volume ratio, that provides a large surface area for cell attachment [16–18].

In the present work, we describe the design, production and characterization of tubes with 4.5 and 1.5 mm inner diameters made of electrospun silk fibroin (ES-SF). Electrospun scaffolds with $ID \leq 1.5$ mm made of PCL [19], a copolymer of ε-caprolactone and L-lactide (PCL/PLA) [20], and blends of PCL and poly-D,L-lactide (PDLLA) [21] are reported in literature. Silk fibroin was already evaluated for the fabrication of small diameter blood vessel grafts [5,22,23], including electrospun tu-bular matrices [24–27]. Soffer et al. [24] fabricated ES-SF tubes with 5 mm *ID* by all-water-based approach; the scaffolds were morphologi-cally, mechanically and biologically characterized in terms of tensile properties, burst strength, creep behavior and *in vitro* test with human vascular cells. Compliant ES-SF tubular scaffolds ($ID = 6$ mm) were developed by Marelli et al. [25]. The circumferential tensile behavior, the burst strength and the compliance of ES-SF tubes were assessed, demonstrating a compliance value higher than Dacron® and Goretex® pros-theses but slightly lower than human saphenous vein [25]. Zhou et al.[26] evaluated the *in vitro* and *in vivo* degradation behavior of aqueous-derived ES-SF scaffolds. The tubes ($ID = 6$ mm) were completely degraded 8 weeks after subcutaneous and intramuscular implantations in male Sprague Dawley rats [26]. Zhou et al. [27] optimized the processing parameters to fabricate ES-SF tubular scaffolds using a concentrated aqueous SF solution; the samples were morphologically and mechanically characterized. However, to the best of our knowledge, this is the first work which has extensively evaluated ES-SF tubes, considering morphological and mechanical aspects, *in vitro* degradation, and *in vitro* and *in vivo* biocompatibility. ES-SF tubular scaffolds with such a small diameter ($ID = 1.5$ mm) are novel SF biomaterial scaffolds, not yet reported in literature, as they were obtained by electrospinning of SF in tubular shape without any other material. They can be used as vascular grafts in pediatrics or in hand microsurgery.

2. Materials and methods

2.1. Materials

Bombyx mori cocoons were kindly supplied by the CRA (Council of Research and Experiments in Agriculture, Apiculture and Sericulture Unit, Padua, Italy). All chemical reagents were obtained from Sigma Aldrich, unless mentioned otherwise.

2.2. Preparation of regenerated Bombyx mori silk fibroin films

SF films, required for the preparation of the solution for the electrospinning process, were prepared as follows. The *Bombyx mori* co-coons were degummed in autoclave at 120 °C for 15 min and then rinsed with distilled water to extract sericin. After drying at room temperature and storing under controlled conditions ($T = 20 \pm 2$ °C, r.h. $= 65 \pm 2\%$), the extracted SF fibers were neutralized to restore the chemical equilibrium of silk fibroin at around its isoelectric point (pI, pI of SF heavy-chain = 4.2 [28]). Briefly, SF fibers were soaked in an aqueous solution of 0.05 M sodium bicarbonate and 1 g/l sodium do-decyl sulfate for 30 min. Then, SF fibers were immersed in an aqueous solution of 0.01 M acetic acid and 0.01 M sodium acetate (0.01 M AA + 0.01 M NaA) for 30 min. Subsequently, SF fibers were soaked again in a 0.01 M AA + 0.01 M NaA for at least 14 h, and finally rinsed with distilled water for 30 min. After degumming and neutralization, and before any subsequent processing, the purity of silk fibroin fibers was checked by optical (colorimetric assay with Blue Comassie) and scanning electron microscopy. After drying at room temperature and storing under controlled conditions as above described, SF fibers were solubilized in a 9.3 M lithium bromide (LiBr) aqueous solution ($T = 60 \pm 2$ °C, $t = 3$ h) to obtain a 10% w/v SF solution. The solution was then diluted with distilled water to obtain a 2% w/v SF concen-tration, and dialyzed against distilled water for 3 days using cellulose membrane dialysis tubing (molecular weight cut-off = 12,000) to eliminate LiBr salts. SF films were prepared by pouring 15 ml of the 2% w/v SF solution into Petri dishes ($\varnothing = 5.5$ cm), followed by cast-ing under fume hood at room temperature until complete solvent evaporation.

2.3. Electrospinning of silk fibroin tubes

A 7.5% w/v SF solution was prepared at room temperature by dissolving SF films in formic acid (98 vol.%) and electrospun with a home-made electrospinning (ES) apparatus. The SF solution was placed in a 10 ml polypropylene syringe and forced by a syringe-pump (KD Sci-entific, KDS 100), at 1.1 ml/h constant volume flow rate, into the spin-neret, a stainless steel capillary tube ($ID = 1.1$ mm). The spinneret was connected to the positive output (+12 kV) of a high voltage power supply (Fug Elektronik GmbH, HCN 35–12,500), while the nega-tive pole (−12 kV) was joined to the fiber collector, to obtain an electric potential difference of 24 kV. The spinneret was moved horizontally by a DC-motor (RS Components) equipped with a linear guide (RS Compo-nents) to allow a more uniform fiber deposition onto the collector. ES-SF tubular scaffolds were prepared using stainless steel mandrels, as rotating collectors (about 2700 rpm), that were placed at 10 cm from the spinneret. ES-SF 4.5 ID and ES-SF 1.5 ID tubes were fabricated using collectors with 4.5 and 1.5 mm diameters, respectively. To fa-cilitate the removal of ES-SF tubes from the mandrels, a sacrificial layer of PEO (200,000 Da) was electrospun on the mandrels before the SF deposition. Briefly, an aqueous PEO solution (7.5% w/v) was electrospun onto the rotating mandrel, placed at 10 cm from the spinneret, using a flow rate and a potential difference equal to 1.1 ml/h and 24 kV, respectively. After overnight drying, SF solution was electrospun onto the mandrels coated with PEO. After the com-plete evaporation of formic acid, ES-SF tubular scaffolds (ES-SF 4.5 ID and ES-SF 1.5 ID) were treated with methanol (>99.9%) for 15 min to induce SF crystallization and partially dissolve PEO, facilitating the ES-SF tube removal from the collectors. Finally, ES-SF tubular scaf-folds were rinsed with distilled water at 37 °C for 48 h, before further characterization.

2.4. Morphological characterization

The wall thickness of the ES-SF tubular scaffolds was measured with a micrometer in three different points for each specimen (n = 3 for each *ID*). The morphology of the two types of ES-SF tubular scaffolds was ob-served by Scanning Electron Microscopy (SEM, Cambridge Instrument Stereoscan 360). The specimens were mounted onto aluminum stubs, gold sputter-coated (Edwards Sputter Coater 5150B) and observed at different magnifications with a 10 kV accelerating voltage. The average fiber diameter was determined from SEM images (5000x) by analyzing 100 electrospun fibers, using ImageJ software (US National Institute of Health).

2.5. Axial and circumferential tensile tests

Axial and circumferential tensile tests were performed on ES-SF 4.5 ID and ES-SF 1.5 ID tubular samples, using a dynamic mechanical ana-lyzer (DMA Q800, TA Instruments).

For axial tensile tests, tubular specimens (n = 3 for each *ID* tubular scaffold, length = 17 mm, gage length = 8 mm) were cut by a scalpel from different ES-SF tubular scaffolds. Samples were imbibed in phos-phate buffered saline (PBS) for 10 min and tested at 37 °C with a preload of 0.005 N and a force ramp of 0.05 N/min until break. Tubular samples were clamped at their cut ends as previously reported in literature [9, 29].

Circumferential tensile tests were performed using home-made *ad hoc* grips made of Nitinol wires (diameter = 0.33 mm) (Fig. 1A). For each kind of tubular scaffold, ring-shaped specimens (n = 3 for each *ID*, axial length = 4 mm) were cut by a scalpel from different ES-SF tubes, imbibed in PBS for 10 min, and tested at 37 °C with a preload of 0.01 N and a force ramp of 0.05 N/min until break.

The following mechanical parameters were drawn from the obtain-ed stress/strain curves: elastic modulus (*E*), ultimate tensile strength (*UTS*), and strain at break (ε_b). *UTS* and ε_b were considered the maxi-mum stress value before failure and its corresponding value of strain, re-spectively. The elastic modulus was calculated using a least-square fitting in the range of 0–25% strain and in the range of 0–8% for axial and circumferential tensile tests, respectively. In addition, for circumfer-ential tensile tests, the curve slope was measured in a second range of strain (8–25%).

2.6. Estimated burst pressure

In accordance to Gauvin et al. [30], the estimated burst pressure (*BP*) was calculated by rearranging the Laplace's law for a pressurized thin-walled hollow cylinder:

$$BP_{estimated} = 2\frac{UTS \cdot t}{ID} \tag{1}$$

where UTS was measured by circumferential tensile tests, t is the wall thickness and *ID* is the unpressurized inner diameter of the ES tubular scaffolds. A graft is defined as thin-walled hollow cylinder when the ratio between its thickness and its diameter is minor than 0.1; therefore, referring to the morphological analysis, ES-SF 4.5 ID and ES-SF 1.5 ID tubular scaffolds can be considered thin-walled hollow cylinders.

2.7. Estimation of tubular scaffold distensibility and compliance

In accordance to Benetos et al. [31], the effect of the distension on the stretching of an artery wall can be evaluated using the distensibility coefficient (*DC*), defined as:

$$DC = 2\frac{{}^{D_s - D_d}/_{D_d}}{\Delta P} \tag{2}$$

where D_s is the systolic diameter, D_d is the diastolic diameter and ΔP is the pulse pressure (systolic minus diastolic blood pressure). This parameter represents the strain of the arterial wall for a given pressure and pertains to the mechanical loading of the artery during a cardiac cycle. In this work, we considered the *DC* for a preliminary estimation of the ES-SF tubular scaffold compliance in the physiological pressure range (80 mm Hg–120 mm Hg). The Laplace's law and the load/displacement curves obtained by circumferential tensile tests were used to calculate the *DC*. The Laplace's law for a pressurized thin-walled hollow cylinder is equal to:

$$\sigma_c = P\frac{ID}{2 \cdot t} \tag{3}$$

where σ_c is the wall stress, *P* is the considered pressure (80 and 120 mm Hg), *ID* is the inner diameter of the ES tubular scaffolds and *t* is the wall thickness. The estimated *DC* of native rat abdominal aorta, harvested from a male Sprague Dawley rat (rat weight = 300 g), and of a Goretex® prosthesis (*ID* = 3.5 mm) were considered as control.

2.8. Determination of suture retention strength

Suture retention strength tests were performed to determine the force necessary to pull a suture from the tubular graft or cause the wall of the graft to fail. In accordance with the standard practice ISO

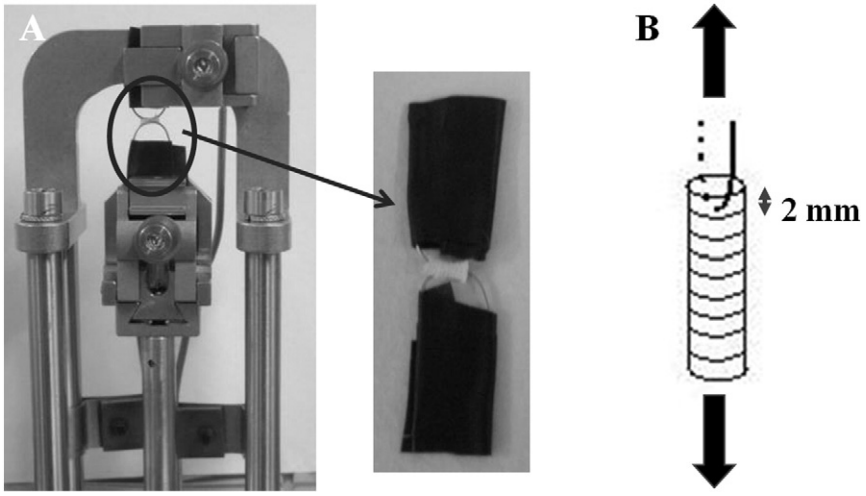

Fig. 1. (A) Custom clamps for circumferential tensile tests. (B) Sketch of the set-up for suture retention strength tests.

7198 "Cardiovascular implants — Tubular vascular prostheses", a suture (8–0 Prolene, Ethicon) was inserted at a distance of 2 mm from the edge of the ES-SF 1.5 ID tubular specimens (length = 15 mm) through the tube wall to form a half loop (Fig. 1B). The 8–0 Prolene suture had the same size of one used for *in vivo* implants of gel spun SF tubes into the rat abdominal aorta (8–0 monofilament Polypropylene suture) [5]. As the only parameter that should influence the suture retention strength of the graft is the wall thickness, we performed the test only on ES-SF 1.5 ID tubes. ES-SF 1.5 ID tubular scaffolds were purposely produced with different wall thickness (ES-SF 1.5A = 40 ± 10 μm, ES-SF 1.5B = 80 ± 15 μm, ES-SF 1.5C = 120 ± 25 μm) to investigate the influ-ence of this parameter on the suture retention strength. Specimens (n = 3 for each considered wall thickness) were imbibed in PBS for 10 min before tests. The suture and the opposite edge of the tubular specimen were fixed in the clamps of a MTS 1 M/H apparatus. Tests were performed at a cross-head displacement rate of 50 mm/min up to pull the suture through the tubular sample or cause the break of the sample wall (ISO 7198). Mean and standard deviation values of su-ture retention strength were calculated for each investigated wall thickness.

2.9. Enzymatic degradation tests

Tubular specimens (~5 mg in weight) were cut by a scalpel from the ES-SF 4.5 ID tubular scaffolds. The larger tube diameter was chosen for this test because of the higher exposed surface available to the enzyme. After 12 h at 20 °C and 60% relative humidity, the specimens were weighed and then sterilized in autoclave at 120 °C for 15 min. A 1 U/ml enzymatic solution of Protease Type XIV from *Streptomyces griseus* was prepared in a buffered solution containing 10 mM sodium acetate and 5 mM calcium acetate (pH 7.5) [32], and sterilized by filtration. Specimens of ES-SF tubes were incubated at 37 °C in protease solution at an enzyme concentration of 0.1 U/mg or in buffer solution (blank). The tests were carried out in triplicate for each time point; enzymatic and buffer solutions were renewed every 3 days. At predetermined time-points (t = 1, 2, 3, 4, 7, 10, 17, 24 days), the specimens were removed from the solutions, treated with hot distilled water (T = 80 °C) for 30 min to inactivate the enzyme (only for the samples extracted from enzymatic solution), rinsed at room temperature in dis-tilled water to remove residuals of salts, and dried overnight at 20 °C and 60% r.h. before further analysis. After incubation in enzymatic or buffered solution, the weight variation (ΔW %) of the ES-SF samples, was calculated at each time-point according to the formula (1):

$$\Delta W\% = \frac{(W_0 - W_t)}{W0} \times 100 \quad (4)$$

where W_0 is the weight at $t = 0$, and W_t is the weight at the time-point t.

The morphology of ES-SF specimens was evaluated by SEM (Jeol JSM-6380 LV). The samples were mounted onto aluminum stubs, gold sputter-coated (Automatic Sputter Coater, Gressington 108 Auto) and observed at different magnifications with a 20 kV accelerating voltage. Crystallinity variation of the ES-SF samples was studied by Fourier transform infrared spectroscopy (FTIR) with a Thermo Nicolet 6700 FT-IR spectrometer, equipped with an attenuated total reflectance (ATR) accessory and ZnSe crystal. Spectra were normalized to the 1446 cm^{-1} peak before any data processing. The FTIR Crystallinity Index (*CI*) was calculated as the intensity ratio between the amide III bands at 1260 cm^{-1} and 1230 cm^{-1} (I_{1260}/I_{1230}) [25,33]. Differential Scanning Calorimetry (DSC) analyses were performed with a Q200 DSC (TA Instruments) using standard aluminum pans. Specimens of about 2–4 mg were heated from 20 up to 500 °C, under N_2 atmosphere, at a 10 °C/min scanning rate. Specifically, the variation of the melting/decomposition peak values, calculated from the DSC thermograms, was assessed during the incubation time. The samples were analyzed in duplicate.

2.10. In vitro cell interaction study

Primary porcine aortic smooth muscle cells (SMCs) were isolated from pigs as previously described [34] and used at passage 4. Briefly, SMCs were isolated from normal 2–4 week-old pigs by a collagenase digestion [34]. The SMCs were cultured in Dulbecco's modified Eagle's medium (DMEM), containing 4.5 g/L glucose (DMEM high glucose) supplemented with 10% fetal bovine serum (FBS, Lonza), 10% porcine serum (Euroclone), 4 mM L-glutamine (Life Technologies), 1% penicillin/streptomycin solution (Life Technologies), 5 mM N-2-hydroxyethylpiperazine-N-2-ethanesulfonic acid (HEPES). For cell expansion, the medium was replaced three-times a week and the cultures were maintained in a humidified incubator at 37 °C and 5% CO_2.

ES-SF 1.5 ID tubular samples (length = 1 cm, n = 3 for each time-point) were sterilized by ethylene oxide and seeded at a density of 1×10^6 cells per sample using a rotating device (Stuart Rotator SB3). The cell suspension (2 ml) was placed in a cryovial and each ES-SF 1.5 ID sample, mounted onto a mandrel, was put inside the vial. Cryovials rotated for 4 h in a humidified incubator to promote cell adhesion on the tubular scaffolds. The ES-SF 1.5 ID scaffolds were then statically cul-tured in 15 ml culture medium, that was replaced every 2 days, for 7 days.

After 3 and 7 days of culture, cell distribution onto ES-SF 1.5 ID tubu-lar scaffolds was evaluated by 3-[4,5-dimethylthiazol-2]-2,5-dipheniltetrazolium bromide (MTT) assay. Cell seeded samples were rinsed with PBS (Invitrogen) and incubated for 3 h at 37 °C with 0.5 mg/ml MTT in sterile DMEM medium without phenol red. After in-cubation, unreacted MTT was removed by rinsing with PBS. Finally, ES-SF samples were observed with an optical microscope (Carl Zeiss) to qualitatively analyze the cell distribution on their surface.

After 7 days of culture, the ES-SF 1.5 ID tubular scaffolds were fixed in Bouin's solution (Diapath) for 4 h at 4 °C, dehydrated in ascending concentrations of alcohol and embedded in paraffin. Sections (3 μm thick) of ES-SF1.5 ID samples were stained with hematoxylin and eosin (H&E) and observed with an optical microscope (Carl Zeiss) to an-alyze the cell distribution in the tube cross-section.

2.11. In vivo subcutaneous implantation

Three male Lewis rats weighting 200–250 g were used for *in vivo* subcutaneous tests. The animals were maintained under standard con-ditions (12 h light:dark cycle, controlled room temperature at 20–22 °C, r.h. >60%) and housed individually with free access to standard pellet diet and water. Animal care and treatment, anesthesia and sacri-fices at the end of the trial were conducted in accordance with institu-tional guidelines that are in compliance with national (n.116, suppl. 40, 18 febbraio 1992, Circolare n.8, 14 luglio 1994) and international (EEC Council Directive 86/609, OJL358-1, Dec. 1987; Guide for the Care and Use of Laboratory Animals, U.S. National Research Council, 1996) guidelines and policies. Ethylene oxide sterilized flat ES-SF spec-imens (10 × 10 mm), cut from different ES-SF 4.5 ID tubes, were im-planted in the dorsal subcutaneous tissue of the rats (Fig. 2). Each sample was fixed to the tissue with a 4.0 silk suture (Ethicon Inc.) to maintain the sample on site. After 15 days the animals were euthana-tized by CO_2 inhalation and the grafts were harvested.

Immediately after the explant, the samples were washed in 0.9% NaCl, immersed for fixation in Bouin's solution (BioOptica) overnight, subsequently dehydrated in graded ethanol series and cleared in tolu-ene (BioOptica), and embedded in paraffin. Microtome sections (5 μm thick) were processed and stained for light microscopy studies. H&E staining was used to assess the tissue integration of the material in the host tissue. The stained sections were observed under a light micro-scope fitted with a digital camera (Olympus).

Immunofluorescence staining was performed to evaluate the pres-ence of host fibroblasts in explanted fibroin and the inflammatory

Fig. 2. ES-SF tubular scaffolds implanted subcutaneously in Lewis male rats for 15 days.

response induced *in vivo* by the ES-SF samples. Briefly, explanted samples were fixed overnight with 4% paraformaldehyde in PBS and frozen in liquid nitrogen. Slides of frozen tissue were incubated with anti actin-α-smooth muscle-Cy3 for fibroblast investigation. For macrophages and T lymphocytes, slides were incubated with primary antibody mouse anti-rat ED1 (Chemicon Int) and goat anti-human CD4 (Santa Cruz Biotechnology, Inc.), respectively. They were then incubated with secondary antibody donkey anti-mouse Cy3 or rabbit anti-goat Cy2 (Jackson ImmunoResearch) for macrophages and T lymphocytes, respectively. Counter staining with DAPI (1 μg/ml) was performed for cell nuclear staining. Stained samples were finally examined by laser confocal microscopy (LSM 510 Meta, Carl Zeiss) at excitation/emission wavelengths of 550/570 nm and 492/510 nm for detecting Cy3 and Cy2, respectively.

2.12. Statistical analysis

Where possible, data were expressed as mean ± standard deviation and statistically compared by two-sample *t*-Test (significance level = 0.05), Origin® Pro v. 8.5 software. Suture retention strength of each investigated wall thickness was statistically compared by One-way ANOVA (significance level = 0.05 and Tukey means comparison), Origin® Pro v. 8.5 software.

3. Results

3.1. Morphological characterization

Nanostructured ES-SF tubular scaffolds were successfully produced with 4.5 and 1.5 mm *ID* (Fig. 3A and B). The wall thickness was 176 ± 14 μm and 44 ± 7 μm, for ES-SF 4.5 ID and ES-SF 1.5 ID, respec-tively. SEM analyses showed a homogeneous random fiber distribution, with fiber diameters in the nanometric range (Fig. 3C and D). Specifical-ly, the average fiber diameter was 547 ± 132 nm and 555 ± 155 nm for ES-SF 4.5 ID and ES-SF 1.5 ID scaffolds, respectively. The fiber size was not significantly different for the two types of scaffolds. Fiber diameter distributions of ES-SF 4.5 ID and ES-SF 1.5 ID tubes are shown in Fig. 3E and F, respectively. The fiber diameters ranged from 350 to 1270 nm for ES-SF 4.5 ID and from 350 to 990 nm for ES-SF 1.5 ID tubes, respectively, with a narrower diameter distribution for ES-SF 1.5 ID samples.

3.2. Mechanical characterization

3.2.1. Tensile axial and circumferential tests

Representative stress–strain curves obtained by tensile axial mechanical tests show a similar behavior for both ES-SF tubes (Fig. 4A). Two different zones could be detected in the stress/strain curves (Fig. 4A). In the first zone ($\varepsilon = 0$–25%), a higher elastic modulus (*i.e.* higher curve slope) is recorded. Comparing ES-SF 4.5 ID with ES-SF 1.5 ID samples (Table 1), only the values of elastic modulus were signif-icantly different ($p < 0.05$).

Representative stress–strain curves obtained by tensile circumferen-tial mechanical tests exhibit a different behavior, depending on ES-SF tube diameter, specifically in the last part ($\varepsilon >$ 60%) of the stress–strain curves (Fig. 4B). In the first part ($\varepsilon < 8\%$, low-strain regime), a similar lin-ear elastic behavior was detected for ES-SF 4.5 ID and ES-SF 1.5 ID, as confirmed by the elastic modulus values ($p > 0.05$, Table 1). In the sec-ond range of strain ($\varepsilon = 8\%$–25%), ES-SF 4.5 ID showed a higher curve slope, hence a higher stiffness, than ES-SF 1.5 ID ($p < 0.05$, Table 1).

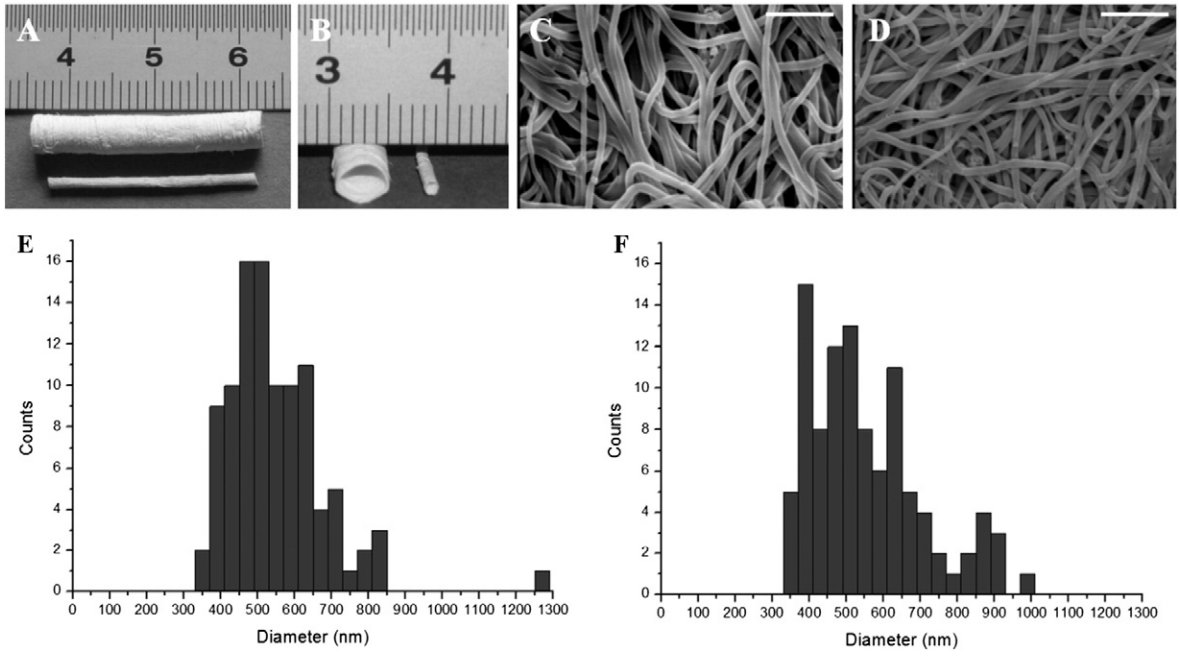

Fig. 3. Macrographs of the length (A) and of the diameter (B) of ES-SF 4.5 ID and ES-SF 1.5 ID tubes. SEM images of ES-SF 4.5 ID (C) and SEM image of ES-SF 1.5 ID (D) tubes (scale bars: 5 μm). Fiber diameter distributions of ES-SF 4.5 ID (E) and ES-SF 1.5 ID (F) tubes.

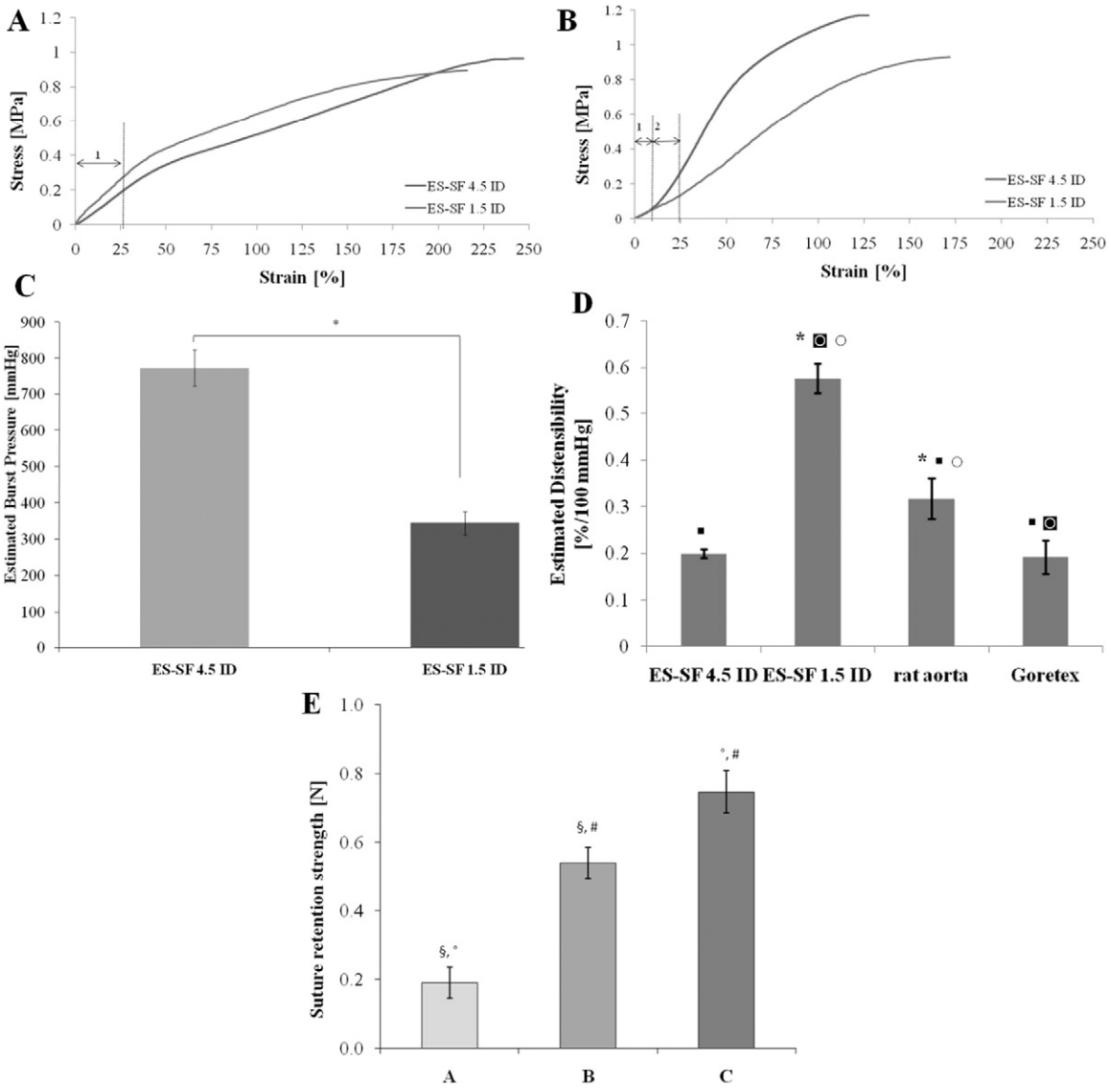

Fig. 4. (A): Representative tensile stress–strain curves of the ES-SF tubular scaffolds obtained by axial tests; the range for the detection of elastic modulus is reported. (B): Representative tensile stress–strain curves of the ES-SF tubular scaffolds obtained by circumferential tests. 1 and 2 indicate the zones considered for detection of elastic modulus and stiffness. (C): Estimated burst pressure evaluated for ES-SF 1.5 ID and ES-SF 4.5 ID tubular scaffolds. (D): Distensibility coefficient (*DC*) considered for a preliminary estimation of the compliance, evaluated for ES-SF 1.5 ID and ES-SF 4.5 ID tubular scaffolds, rat aorta and Goretex® prosthesis; $p < 0.05$ * relative to ES-SF 4.5 ID tubes, ▪ relative to ES-SF 1.5 ID tubes, relative to rat aorta, ○ relative to Goretex prosthesis. (E): Suture retention strength measured for the ES-SF 1.5 ID samples with different wall thickness; §, °, # statistical significance ($p < 0.05$) between A and B, A and C, B and C, respectively.

Specifically, the slope of σ/ε curves for ES-SF 1.5 ID remained similar with $\varepsilon = 0$–25% ($p > 0.05$, Table 1); in contrast, ES-SF 4.5 ID samples exhibited a significant change of the σ/ε slope ($p < 0.05$, Table 1). Then, in the last part of the σ/ε curves ($\varepsilon > 60\%$), there was a decrease of slope (Fig. 4B). Comparing the two ES-SF tubes, strain at break, ultimate tensile strength and stiffness (in the zone of $\varepsilon = 8$–25%) were significantly different ($p < 0.05$, Table 1).

Table 1
Mean and standard deviation values of the considered mechanical parameters obtained by axial and circumferential tensile tests for ES-SF 4.5 ID and ES-SF 1.5 ID scaffolds. (*) = $p < 0.05$.

		ES-SF 4.5 ID	ES-SF 1.5 ID
Axial tensile test	Elastic modulus [MPa] (*)	0.61 ± 0.15	1.33 ± 0.37
	Ultimate tensile strength [MPa]	0.83 ± 0.13	0.95 ± 0.09
	Strain at break [%]	224 ± 29	199 ± 16
Circumferential tensile test	Elastic modulus ($\varepsilon = 0$–8%) [MPa]	0.55 ± 0.01	0.43 ± 0.10
	Stiffness ($\varepsilon = 8$–25%) [MPa] (*)	1.37 ± 0.04	0.41 ± 0.11
	Ultimate tensile strength [MPa] (*)	1.24 ± 0.06	0.90 ± 0.07
	Strain at break [%] (*)	141 ± 19	210 ± 33

3.2.2. Estimation of burst pressure

The burst pressure was estimated from the stress/strain curves obtained in the tensile circumferential tests. A significant difference ($p < 0.05$, Fig. 4C) was observed in the burst pressure of ES-SF 4.5 ID (773 ± 51 mm Hg) compared to ES-SF 1.5 ID (344 ± 32 mm Hg), being higher for the first one.

3.2.3. Estimation of distensibility

The compliance was estimated by the distensibility coefficient (*DC*); in particular, *DC* of rat aorta was higher than that of Goretex® prosthe-sis, while the *DC* value of ES-SF 4.5 ID tubes was lower than that of ES-SF 1.5 ID tubes ($p < 0.05$, Fig. 4D), that showed the highest *DC* value ($p < 0.05$, Fig. 4D).

3.2.4. Suture retention strength

As expected, the suture retention strength increased by increasing the wall thickness of the ES-SF 1.5 ID scaffolds (Fig. 4E). The difference of the retention strength values was significant ($p < 0.05$) among all the considered samples.

3.3. Enzymatic degradation tests

The degradation rate of ES-SF tubular scaffolds incubated with pro-tease followed a linear trend during all the test time; the weight loss at the end of the test ($t = 24$ days) was about 35% of the initial weight (Fig. 5A). As expected, the blank ES-SF samples, incubated only in buffer solution, did not show any weight variation (Fig. 5A).

SEM images (Fig. 5B (a), (b), (c)) show an increase in surface rough-ness and the appearance of cracks in the electrospun nanofibers of the ES-SF tubular scaffolds, by increasing the incubation time in the enzy-matic solution (3, 7 and 17 days of incubation). On the other hand, the blank sample incubated up to 17 days in buffer solution only (Fig. 5B (d)) still revealed well defined and smooth fibers with no sign of surface degradation.

FTIR-ATR analysis assessed the possible changes in surface structure and molecular conformation of SF as a function of the degradation time for ES-SF samples treated with the enzymatic solution, compared to the blank (after 17 days of incubation) and untreated samples. The untreat-ed samples were not incubated in enzymatic or buffer solutions.

The FTIR spectra reported in Fig. 6A indicate that all ES-SF samples maintained the typical β-sheet structure of untreated SF nanofibers, independently from the incubation time and the presence or not of the protease. This is confirmed by the presence of the typical β-sheet bands of the amide I (1699 cm^{-1} and 1626 cm^{-1}), amide II (1518 cm^{-1}), and amide III (1260 cm^{-1} and 1230 cm^{-1}).

To investigate possible crystallinity changes at the surface of ES-SF tubular scaffolds, the Crystallinity Index ($CI = I_{1230/1260}$) was calculated and plotted as a function of the degradation time (Fig. 6B). Both blank and degraded samples displayed a sharp increase of the *CI* value after 1 and 2 days of incubation in buffer and enzymatic solutions,

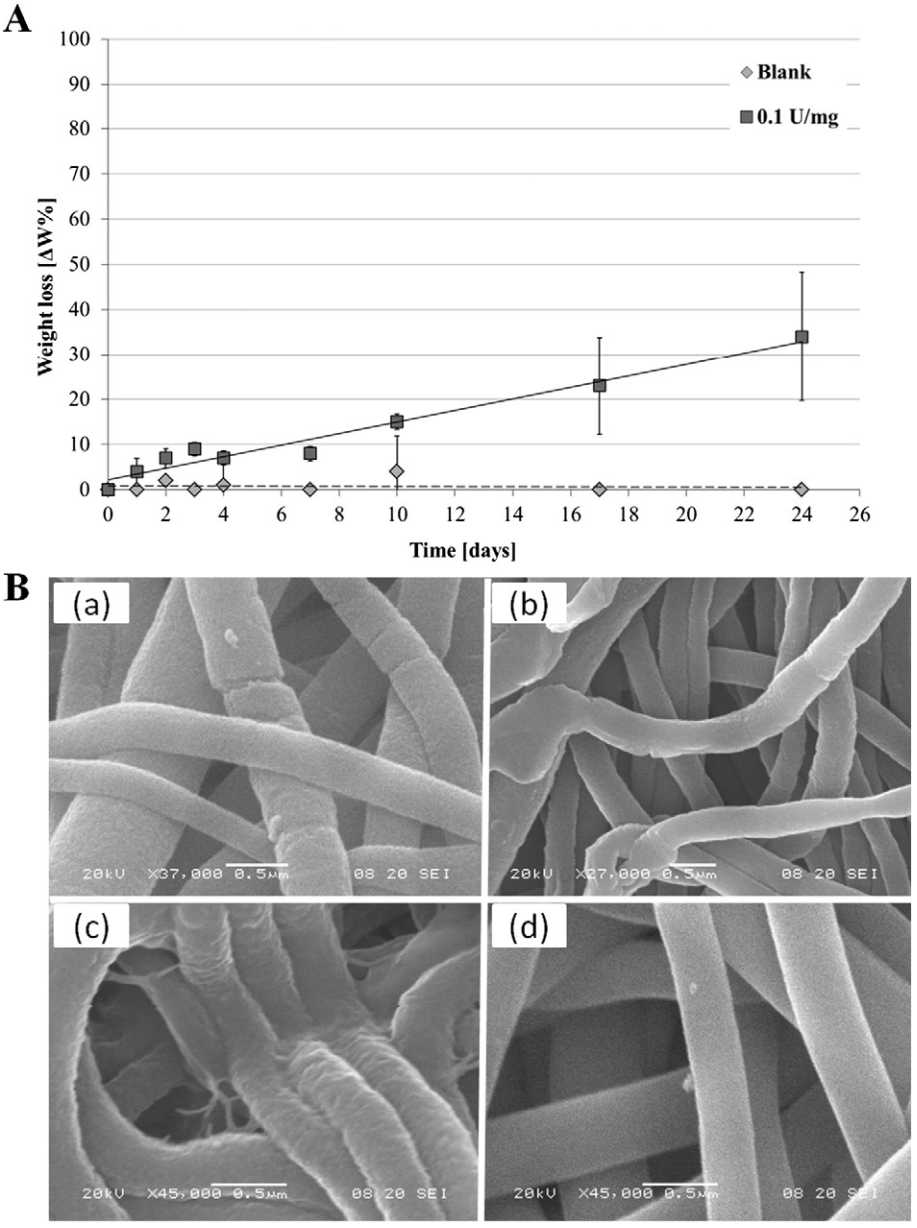

Fig. 5. (A): Percentage of weight loss of ES-SF tubes incubated in the enzyme (protease XIV) solution at 37 °C; blank: ES-SF samples incubated in buffer solution. (B): SEM images of ES-SF tubes incubated in the protease XIV solution at 37 °C after 3 days (a), 7 days (b), 17 days (c), and blank sample after 17 days of incubation in buffer solution (d) (scale bar: 0.5 μm).

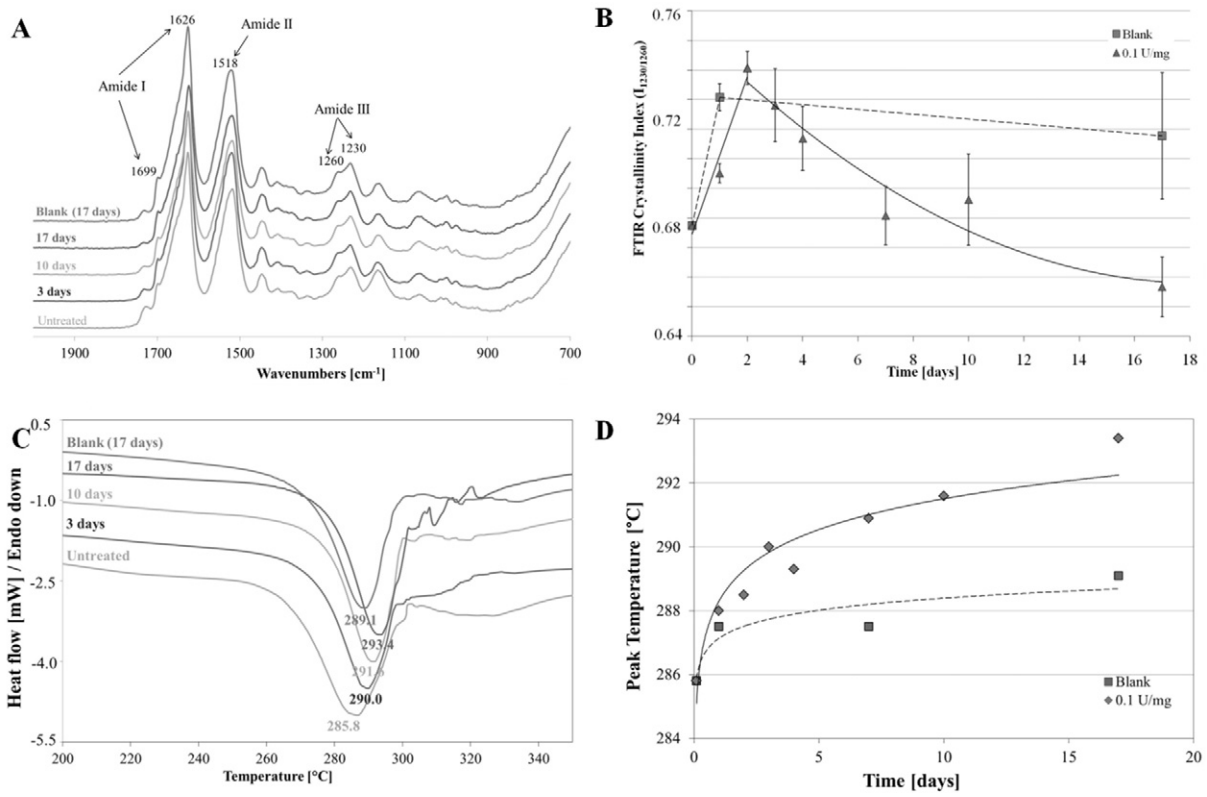

Fig. 6. (A): ATR-FTIR spectra of ES-SF tubes incubated in the protease solution at 37 °C for 3, 10, and 17 days; the blank sample at 17 days was incubated in buffer solution; spectra were compared to the one of untreated ES-SF tubular scaffold. (B): Time dependence of the FTIR Crystallinity Index of ES-SF tubes incubated in the protease solution at 37 °C. (C): DSC thermograms of ES-SF tubes incubated in the protease solution at 37 °C for 3, 10, and 17 days; the blank sample at 17 days was incubated in buffer solution; thermograms were compared to the one of untreated ES-SF tubular scaffold. (D): Time dependence of the temperature of the melting/decomposition peak of ES-SF tubes incubated in the protease solution at 37 °C. Blank refers to samples incubated in buffer solution.

respectively. Afterwards, the *CI* of blank samples remained constant ($p > 0.05$), in contrast the *CI* of protease degraded samples displayed an exponential decay ($p < 0.05$).

Bulk structural properties of ES-SF tubes incubated in buffer and enzymatic solutions were investigated by DSC analysis (Fig. 6C). The strong melting/decomposition endotherm peak at 285.8 °C in untreated SF nanofibers is typical of regenerated SF materials with β-sheet structure [35]. By increasing the degradation time, the endotherm peak shifted to higher temperature and became sharper (Fig. 6C), thus indicating a more ordered arrangement of the SF chains in the bulk of the material upon immersion in protease solution (Fig. 6C). An initial sharp increase of peak temperature was detected for both blank and protease degraded samples (Fig. 6D). Then, a plateau was attained at lower temperature for blank samples and at higher values for the protease treated samples, probably due to the enzymatic cleavage of less ordered SF domains (Fig. 6D).

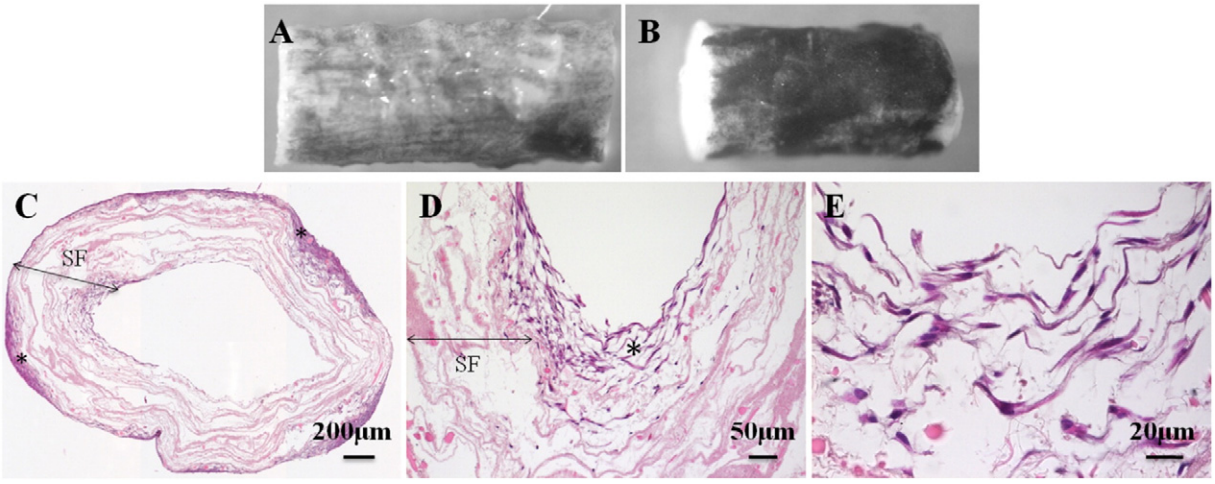

Fig. 7. Qualitative images of MTT assay performed on seeded ES-SF tubes after 3 days (A), and after 7 days (B). (C, D, E): H&E performed on seeded ES-SF 1.5 ID tubes after 7 days: (C) cross section of ES-SF tube (original magnification 10x), (D and E) high magnification of cells on the inner lumen of the scaffolds (original magnification 20× and 63×). Asterisks indicate the presence of SMCs.

3.4. In vitro cell interaction study

MTT assay demonstrated a homogenous SMC distribution after 3 days and 7 days, as reported in Fig. 7A and B.

H&E staining confirmed the qualitative results obtained by the MTT assay; ES-SF 1.5 ID tubes showed a homogenous cell distribution on the outer surface, with the presence of a thin cell layer (Fig. 7C). Further-more, there were some cells in the tube wall thickness (Fig. 7D and E). Cells were able to migrate from the tube outer surface to the lumen, however the cell distribution into the tube thickness was heteroge-neous (Fig. 7D and E).

3.5. In vivo subcutaneous implantation

At 15 days after subcutaneous implantation in Lewis rats, histological analysis demonstrated a good integration of the grafts in the host tis-sue, showing the presence of a thin fibrotic cellular overgrowth around the implant (Fig. 8A). The fibrotic capsule was characterized by the presence of fibroblasts as shown by immunofluorescence analyses of explanted grafts (Fig. 2B); however, host cells were able to overcome the fibrotic capsule and homogeneously colonize the ES-SF samples (Fig. 8A).

Immunofluorescence analyses of explanted grafts showed a low inflammatory response (Fig. 8C). Few inflammatory macrophages, stained with anti-ED1 antibody, were observed in the fibrotic capsule and in scaffolds retrieved from the animals, indicating a low inflamma-tory reaction (Fig. 8C). Furthermore, T lymphocytes, stained with anti-CD4 antibody, were completely absent, demonstrating no immune re-action caused by the implanted samples (Fig. 8C).

4. Discussion

The use of a scaffold that mimics the native structure of the ECM plays a fundamental role in tissue regeneration. For this reason, in the present study, tubular scaffolds of SF were obtained by electrospinning, thus combining the typical morphological properties of electrospun mats with the good biocompatibility, excellent mechanical properties and versatile processability of SF. Furthermore, ES-SF tubular scaffolds with 1.5 mm *ID* were produced for the first time by electrospinning of SF alone, and characterized for a possible application as small diameter grafts to be used in pediatrics and in hand microsurgery. In our previous work [36], *in vivo* functionality tests of acellular ES-SF 1.5 ID tubes implanted in the abdominal aorta of Lewis rats for 7 days showed no signs of acute thrombosis and occlusion, and the absence of aneurismal dilatation and apparent intimal hyperplasia. Even after a short period of implantation, ES-SF 1.5 ID tubular scaffolds allowed the regeneration of neo-tissue similar to the native blood vessels; in fact histological and immunofluorescence analysis detected the presence of SMCs, endothelial cells (ECs), elastin and blood capillaries [36]. ES-SF tubular scaffolds induced elastin regeneration which was observed only with few other tissue engineered vascular grafts [2]. In contrast, previous experiments performed by other research groups with different SF scaffold forms (*i.e.* gel spun tubes [5], woven thread tubes [22] and knitted tubes [23]) did not show elastin deposition in the graft lumen. The reason for the favorable results obtained with our ES-SF tubular scaffolds can be attributed to the combination of the excellent biocompatibility and mechanical properties of SF and the nanostructured morphology obtained by electrospinning.

The ES-SF 4.5 ID and ES-SF 1.5 ID tubular scaffolds were made of nanofibers with a homogeneous random fiber distribution. SEM observations showed a random fiber distribution, as the tubular scaffolds were fabricated with a collector rotation rate of about 2700 rpm, corresponding to a collector tangential speed (about 0.65 m/s and about 0.20 m/s for ES-SF 4.5 ID and ES-SF 1.5 ID, respectively) not adequate, *i.e.* too low to allow the circumferential fibers alignment. To obtain fiber alignment in a circumferential manner onto the cylinder surface, the tangential speed has to exceed the fiber delivery rate (tangential speed ≥ 2–2.5 m/s [37,38]). However, the random nanofiber distribution of ES-SF 1.5 ID tubes showed an appropriate morphology for a good interaction with primary porcine SMCs and for the regeneration of vessel-like structure [36].

Concerning the mechanical properties, only ES-SF 4.5 ID tubular scaffolds showed significantly higher ultimate tensile strength (*UTS*) and lower strain at break obtained by circumferential tensile tests

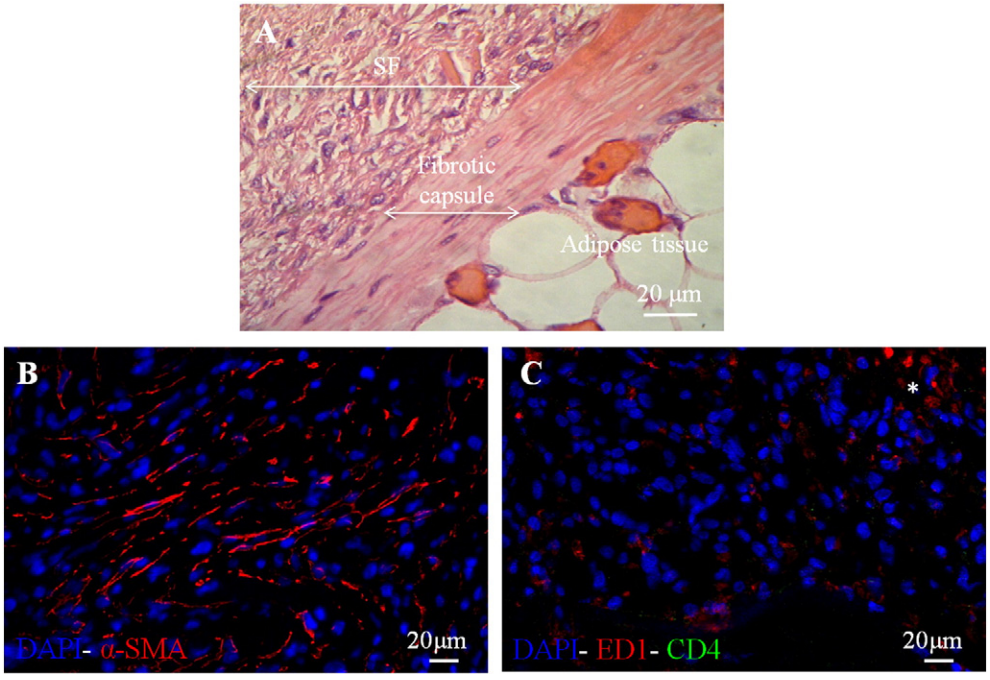

Fig. 8. ES-SF tubular scaffolds implanted subcutaneously in Lewis male rats for 15 days. (A) Histological image by H&E staining of ES-SF samples at 15 days after implantation. (B, C) Immunofluorescence analysis of fibroblasts (red, B), macrophages (*, red, C), and T lymphocytes (green, C); magnification 40×.

than those measured by axial tensile tests, indicating anisotropic prop-erties of the scaffolds. The anisotropic mechanical behavior may be re-lated to a slight different fiber orientation in the tube wall. In comparison to ES-SF 1.5 ID tubular scaffolds, the anisotropic behavior of ES-SF 4.5 ID tubes may be affected by different collector tangential speed (about 0.65 m/s and about 0.20 m/s for ES-SF 4.5 ID and ES-SF 1.5 ID, respectively) and electric field, due to the different collector diameter.

Substitutes for blood vessel regeneration must demonstrate adequate mechanical properties. ES-SF tubular scaffolds are here compared with electrospun scaffolds made of a synthetic polymer, PCL, that is widely used for vascular tissue engineering applications, and a natural polymer, elastin, that is one of the major ECM proteins in the arterial wall. ES-SF tubes exhibited higher *UTS* and strain at break than electrospun tropoelastin scaffolds, but lower than electrospun PCL scaf-folds (Table 2). This comparison demonstrated that ES-SF tubular scaf-folds showed higher mechanical properties than another natural polymer, but lower than a synthetic polymer. Specifically, ES-SF tubes showed higher elongation than elastin, that usually exhibits great elon-gation. ES-SF tubes exhibited higher elongation than electrospun SF mats (Table 2). The reason for the higher elongation of the tubes can be attributed to the wet condition of our samples, instead of dry condi-tion of electrospun SF mats [39]. In fact, the plasticizing effect of water allows the greater elongation of ES-SF tubular scaffolds. Furthermore, the wet condition of our tests mimicked the human body environment better.

ES-SF tubes showed higher *UTS* in circumferential direction than na-tive anterior descending human coronary arteries and higher strain at break than human saphenous veins, the gold standard for arterial by-pass grafts, in both directions (Table 2). Therefore, ES-SF tubes demon-strated appropriate tensile mechanical properties for small diameter blood vessel regeneration.

Due to the permeability of the ES-SF tubes at pressures higher than 80 mm Hg [25], in a previous work [25] a highly deformable balloon was inflated inside the sample under a controlled pressure for the measurement of the compliance and the burst pressure, in accordance with the ISO 7198. Considering the very small internal diameter of the ES-SF 1.5 ID scaffolds, it was impossible to experimentally measure their compliance and burst pressure, since no balloon with the adequate properties was commercially available. For this reason, in this work the burst pressure and distensibility of ES-SF tubular scaffolds were theoretically estimated. The distensibility coefficient can be used also as a preliminary estimation of the ES-SF tubular scaffold compliance. The *DC* of native rat aorta was significantly higher than that of Goretex® prosthesis ($p < 0.05$), as previously reported [3].The*DC* of ES-SF 1.5 ID tubular scaffolds was significantly higher than that of Goretex® prosthesis and native rat aorta ($p < 0.05$), demonstrating an adequate behavior for blood vessel regeneration. Specifically, the *DC* of ES-SF 1.5 ID tubes and native rat aorta was equal to 0.58 ± 0.03%/100 mm Hg and 0.32 ± 0.04%/100 mm Hg, respectively. However, the used method underestimates the *DC* of native rat aorta, since the rat aorta is not a thin-walled hollow cylinder; in fact the ratio between the thickness and the diameter is equal to 0.126, which is slightly higher than the reference value (0.1 [43]). ES-SF 4.5 ID tubular scaffolds exhibited similar DC (0.20 ± 0.01%/100 mm Hg) to native rat aorta and Goretex® prosthesis ($p > 0.05$), but significantly lower than ES-SF 1.5 ID tubes ($p < 0.05$). The different *DC* between ES-SF 4.5 ID and ES-SF 1.5 ID tubes may be related to a slight different fiber orientation in the scaffold wall. The burst pres-sure of the two different *ID* tubes was estimated and it was comparable with the burst pressure of electrospun SF tubes, experimentally mea-sured in other studies as 811 mm Hg and 575 mm Hg, respectively [24,25]. These studies used different solutions for SF electrospinning (an aqueous blend of SF and PEO [24] and a solution of SF and formic acid [25]) and different systems for measuring the burst pressure that could be the causes of the different burst pressure values reported. Fur-thermore, the ES-SF tubes developed in this study bore up to a pressure value higher than the upper pathological pressures (180–220 mm Hg), but lower than native human saphenous veins (~2000 mm Hg [44]). However, preliminary *in vivo* functionality tests showed no mechanical issues of the ES-SF grafts [36]. Furthermore, ES-SF grafts showed a fast regeneration of the vessel-like structure [36] that may allow the support of *in vivo* mechanical loading.

The suture retention strength (*SRS*) value of the thickest ES-SF 1.5 ID tubular scaffolds (wall thickness = 120 ± 25 μm) was appropriate for the specific application, in fact the value was similar to that of native in-ternal mammary artery (0.76–2.01 N [45]). Furthermore, the *SRS* values of ES-SF 1.5 ID tubes (wall thickness = 80 ± 15 μm and 120 ± 25 μm) were higher than those of other natural polymer-based scaffolds, such as fibrin gel. Fibrin gels with embedded cells exhibited a *SRS* value equal to 0.19 ± 0.05 N, that were obtained by applying a lower cross-head displacement rate (2 mm/min) [12] than the value range indicated in the ISO 7198. Although fibrin gels were *in vitro* conditioned to en-hance the cells alignment, the *SRS* of fibrin gels was lower than that of ES-SF tubes. Electrospun PCL tubes exhibited higher *SRS* values (4.8–9.18 N [9,10]) than those of ES-SF 1.5 ID. However, the *SRS* values of ES-SF 1.5 ID (wall thickness = 80 ± 15 μm) were similar to that of PGS porous tubes coated with electrospun PCL (0.45 ± 0.031 N applying a crosshead displacement rate of 2 mm/min [8]). PGS-PCL scaffolds showed an excellent biological behavior as interposition grafts in rat ab-dominal aorta for 3 months [8], demonstrating an appropriate SRS value during the *in vivo* implants. Therefore, also the SRS of ES-SF 1.5 ID tubu-lar scaffolds (wall thickness = 80 ± 15 μm) should be appropriate for the *in vivo* characterization, as demonstrated by the *in vivo* implantation in the rat model for 7 days [36].

ES-SF tubes displayed a degradation kinetic similar to other regener-ated SF materials, like films (weight loss = 45.5%, after 17 days) [46], with a rate significantly higher than that of natural SF fibers (weight loss of about 7% [32] or about 2% [46], after 17 days). The increase of the crystallinity index value at short incubation time can be attributed to the quenching effect of the water treatment on SF chains which attained a more ordered crystalline structure on wetting and subse-quent drying. By increasing the exposition time to protease, the external SF layers underwent a decrease of order and crystallinity, as demon-strated by FTIR and SEM analysis. As a consequence of the protease ac-tivity, the nanofibers were attacked from the outside; in fact DSC analysis showed an increase of the crystallinity of the bulk ES-SF tubes due to the digestion and a decrease of amorphous regions, confirming the surface degradation of the ES-SF tubes. Zhou et al. [26] studied the degradation behavior of aqueous-derived electrospun SF tubes using Protease XIV. About 65% of the electrospun SF scaffolds was degraded within 24 days in the enzymatic solution [26] with an enzyme/substrate ratio equal to 0.06 U/mg. These scaffolds demonstrated a faster

Table 2
Mechanical properties of ES-SF tubular scaffold, other electrospun scaffolds and native blood vessels.

Graft	*UTS* [MPa]	ε_b [%]	Reference
ES-SF 4.5 ID	1.24 ± 0.06 [c]	141 ± 19 [c]	This study
	0.83 ± 0.13 [a]	224 ± 29 [a]	
ES-SF 1.5 ID	0.90 ± 0.07 [c]	210 ± 33 [c]	This study
	0.95 ± 0.09 [a]	199 ± 16 [a]	
Electrospun tropoelastin	0.34 ± 0.14 [c]	79 ± 6 [c]	[11]
	0.38 ± 0.05 [a]	75 ± 5 [a]	
Electrospun PCL	4.0 ± 0.4 [a]	140 ± 13 [a]	[40]
	4.1 ± 0.5 [a]	1092 ± 28 [a]	[10]
Electrospun SF mats	18.93 ± 2.64 [*]	16.5 ± 3.6	[39]
	16.03 ± 1.52 [○]	21.7 ± 4.3	
	11.43 ± 2.05 [#]	23.1 ± 4.7	
Human coronary artery	0.39 ± 0.07 [c]	–	[41]
Human saphenous vein	3.01 ± 1.91 [c]	11 ± 5 [c]	[42]
	13.22 ± 5.73 [a]	17 ± 10 [a]	

[c]: circumferential, [a]: axial, [*]: mean fiber diameter = 85.5 nm, [○]: mean fiber diameter = 165.3 nm, [#]: mean fiber diameter = 206.8 nm.

degradation kinetics than ES-SF tubes developed in this study that showed a weight loss of about 35% after 24 days with an enzyme/substrate ratio equal to 0.1 U/mg. Probably, the different degradation behavior of our ES-SF scaffolds compared to the Zhou's work may be correlated to the SF regeneration procedure, specifically Zhou's electrospun SF tubes were fabricated following an all-aqueous process. In fact, Wang et al. [47] demonstrated that *in vivo* degradation kinetic of aqueous-derived SF scaffolds was faster than HFIP-derived SF scaffolds.

The *in vitro* cytocompatibility of ES-SF tubes was confirmed by the adhesion and growth of SMCs onto the ES-SF 1.5 ID tubular scaffolds. In some cases, the porosity of electrospun scaffolds may limit or not allow the cell infiltration inside the scaffold [16,48]. ES-SF 1.5 ID tubes, seeded using a rotational method, exhibited a homogenous cell distribution onto the external surface and a heterogeneous distribution in the tube wall thickness.

In vivo subcutaneous implants showed the presence of few macrophages, demonstrating a low physiological inflammatory reaction of the recipient to the implanted material at 15 days after implantation, demonstrating the complete evaporation of formic acid, the toxic solvent used for electrospinning. The absence of T lymphocytes demonstrated no cell-mediated immunoresponse. As expected, these data confirm the good *in vivo* biocompatibility of SF scaffolds; actually, SF is widely used for tissue engineering applications. At 15 days after implantation, the H&E analysis exhibited the formation of a thin fibrotic capsule mainly populated by fibroblasts, suggesting the completion of the host response to the implant. As shown by H&E analysis and macroscopic evaluation of explanted ES-SF tubes (data not reported), ES-SF tubes remained stable with shape maintenance in a subcutaneous environment for 15 days.

5. Conclusions

Nanostructured tubular scaffolds with inner diameter of 4.5 mm and 1.5 mm were successfully fabricated by electrospinning a solution of SF in formic acid. The *in vitro* characterization of the ES-SF tubular scaffolds performed in this study provided promising results in terms of morphological, mechanical, biological and biodegradation behavior for their possible use as off-the-shelf scaffolds for the regeneration of small diameter blood vessels. Specifically, ES-SF tubular scaffolds showed a random fiber distribution in the nanometric range, allowing the *in vitro* adhesion and growth of primary porcine SMCs. ES-SF tubular scaffolds exhibited appropriate mechanical performance, in terms of axial and circumferential tensile properties, suture retention strength, burst pressure and distensibility. These promising results were confirmed by *in vivo* functionality tests in the abdominal aorta of Lewis rats for 7 days, performed in our previous work [36], where acellular ES-SF 1.5 ID tubular scaffolds allowed the regeneration of neo-tissue similar to the native blood vessels.

Acknowledgments

The work was supported by Cariplo Foundation funds to G. Freddi (Project No. 2007–5457). The authors would like to thank Dr. Francesco Migliavacca, Dr. Lina Altomare and Dr. Giancarlo Pennati for the useful discussion on mechanical analysis.

References

[1] A. Rathore, M. Cleary, Y. Naito, K. Rocco, C. Breuer, Wires Nanomed. Nanobiotechnol. 4 (2012) 257–272.
[2] D. Pankajakshan, D.K. Agrawal, Can. J. Physiol. Pharmacol. 88 (2010) 855–873.
[3] V. Catto, S. Farè, G. Freddi, M.C. Tanzi, ISRN Vasc. Med. 2014 (2014) 1–27.
[4] A. Hasan, A. Memic, N. Annabi, M. Hossain, A. Paul, M.R. Dokmeci, F. Dehghani, A. Khademhosseini, Acta Biomater. 10 (2014) 11–25.
[5] M. Lovett, G. Eng, J.A. Kluge, C. Cannizzaro, G. Vunjak-Novakovic, D.L. Kaplan, Organ-ogenesis 6 (2010) 217–224.
[6] A.F. Pellegata, M.A. Asnaghi, I. Stefani, A. Maestroni, S. Maestroni, T. Dominioni, S. Zonta, G. Zerbini, S. Mantero, BioMed Res. Int. 2013 (2013) 8.
[7] S.W. Cho, I.K. Kim, J.M. Kang, K.W. Song, H.S. Kim, C.H. Park, K.J. Yoo, B.S. Kim, Tissue Eng. A 15 (2009) 901–912.
[8] W. Wu, R.A. Allen, Y. Wang, Nat. Med. 18 (2012) 1148–1153.
[9] S. de Valence, J.C. Tille, J.P. Giliberto, W. Mrowczynski, R. Gurny, B.H. Walpoth, M. Moller, Acta Biomater. 8 (2012) 3914–3920.
[10] S. de Valence, J.C. Tille, D. Mugnai, W. Mrowczynski, R. Gurny, M. Moller, B.H. Walpoth, Biomaterials 33 (2012) 38–47.
[11] K.A. McKenna, M.T. Hinds, R.C. Sarao, P.C. Wu, C.L. Maslen, R.W. Glanville, D. Babcock, K.W. Gregory, Acta Biomater. 8 (2012) 225–233.
[12] Z.H. Syedain, L.A. Meier, J.W. Bjork, A. Lee, R.T. Tranquillo, Biomaterials 32 (2011) 714–722.
[13] G.H. Altman, F. Diaz, C. Jakuba, T. Calabro, R.L. Horan, J. Chen, H. Lu, J. Richmond, D.L. Kaplan, Biomaterials 24 (2003) 401–416.
[14] L.S. Wray, X. Hu, J. Gallego, I. Georgakoudi, F.G. Omenetto, D. Schmidt, D.L. Kaplan, J. Biomed. Mater. Res. B Appl. Biomater. 99 (2011) 89–101.
[15] D.N. Rockwood, R.C. Preda, T. Yucel, X. Wang, M.L. Lovett, D.L. Kaplan, Nat. Protoc. 6 (2011) 1612–1631.
[16] R.L. Dahlin, F.K. Kasper, A.G. Mikos, Tissue Eng. B Rev. 17 (2011) 349–364.
[17] Y. Zhang, C.T. Lim, S. Ramakrishna, Z.M. Huang, J. Mater. Sci. Mater. Med. 16 (2005) 933–946.
[18] S.G. Kumbar, R. James, S.P. Nukavarapu, C.T. Laurencin, Biomed. Mater. 3 (2008) 034002.
[19] F. Kuwabara, Y. Narita, A. Yamawaki-Ogata, M. Satake, H. Kaneko, H. Oshima, A. Usui,
Y. Ueda, J. Artif. Organs 15 (2012) 399–405.
[20] W. He, Z. Ma, W.E. Teo, Y.X. Dong, P.A. Robless, T.C. Lim, S. Ramakrishna, J. Biomed. Mater. Res. A 90 (2009) 205–216.
[21] D. Zhang, J. Chang, Nano Lett. 8 (2008) 3283–3287.
[22] S. Enomoto, M. Sumi, K. Kajimoto, Y. Nakazawa, R. Takahashi, C. Takabayashi, T. Asakura, M. Sata, J. Vasc. Surg. 51 (2010) 155–164.
[23] T. Yagi, M. Sato, Y. Nakazawa, K. Tanaka, M. Sata, K. Itoh, Y. Takagi, T. Asakura, J. Artif. Organs 14 (2011) 89–99.
[24] L. Soffer, X. Wang, X. Zhang, J. Kluge, L. Dorfmann, D.L. Kaplan, G. Leisk, J. Biomater. Sci. Polym. Ed. 19 (2008) 653–664.
[25] B. Marelli, A. Alessandrino, S. Fare, G. Freddi, D. Mantovani, M.C. Tanzi, Acta Biomater. 6 (2010) 4019–4026.
[26] J. Zhou, C. Cao, X. Maa, L. Hua, L. Chen, C. Wang, Polym. Degrad. Stab. 95 (2010) 1679–1685.
[27] J. Zhou, C. Cao, X. Ma, Int. J. Biol. Macromol. 45 (2009) 504–510.
[28] A.E. Terry, D.P. Knight, D. Porter, F. Vollrath, Biomacromolecules 5 (2004) 768–772.
[29] J. Stitzel, J. Liu, S.J. Lee, M. Komura, J. Berry, S. Soker, G. Lim, M. Van Dyke, R. Czerw, J.J. Yoo, A. Atala, Biomaterials 27 (2006) 1088–1094.
[30] R. Gauvin, M. Guillemette, T. Galbraith, J.M. Bourget, D. Larouche, H. Marcoux, D. Aube, C. Hayward, F.A. Auger, L. Germain, Tissue Eng. A 17 (2011) 2049–2059.
[31] A. Benetos, S. Laurent, A.P. Hoeks, P.H. Boutouyrie, M.E. Safar, Arterioscler. Thromb. 13 (1993) 90–97.
[32] R.L. Horan, K. Antle, A.L. Collette, Y. Wang, J. Huang, J.E. Moreau, V. Volloch, D.L. Kaplan, G.H. Altman, Biomaterials 26 (2005) 3385–3393.
[33] G. Freddi, G. Pessina, M. Tsukada, Int. J. Biol. Macromol. 24 (1999) 251–263.
[34] C. Arrigoni, A. Chitto, S. Mantero, A. Remuzzi, Biotechnol. Bioeng. 100 (2008) 988–997.
[35] A. Motta, L. Fambri, C. Migliaresi, Macromol. Chem. Phys. 203 (2002) 1658–1665.
[36] I. Cattaneo, M. Figliuzzi, N. Azzollini, V. Catto, S. Fare, M.C. Tanzi, A. Alessandrino, G. Freddi, A. Remuzzi, Int. J. Artif. Organs 36 (2013) 166–174.
[37] T. Courtney, M.S. Sacks, J. Stankus, J. Guan, W.R. Wagner, Biomaterials 27 (2006) 3631–3638.
[38] C.H. Lee, H.J. Shin, I.H. Cho, Y.M. Kang, I.A. Kim, K.D. Park, J.W. Shin, Biomaterials 26 (2005) 1261–1270.
[39] N. Amiraliyan, M. Nouri, M.H. Kish, Polym. Sci. Ser. A 52 (2010) 407–412.
[40] S.J. Lee, J. Liu, S.H. Oh, S. Soker, A. Atala, J.J. Yoo, Biomaterials 29 (2008) 2891–2898.
[41] E. Claes, J.M. Atienza, G.V. Guinea, F.J. Rojo, J.M. Bernal, J.M. Revuelta, M. Elices, Conf. Proc. IEEE Eng. Med. Biol. Soc. 2010 (2010) 3792–3795.
[42] D.L. Donovan, S.P. Schmidt, S.P. Townshend, G.O. Njus, W.V. Sharp, J. Vasc. Surg. 12 (1990) 531–537.
[43] J.R. Basford, Arch. Phys. Med. Rehabil. 83 (2002) 1165–1170.
[44] M. Peck, D. Gebhart, N. Dusserre, T.N. McAllister, N. L'Heureux, Cells Tissues Organs 195 (2012) 144–158.
[45] G. Konig, T.N. McAllister, N. Dusserre, S.A. Garrido, C. Iyican, A. Marini, A. Fiorillo, H. Avila, W. Wystrychowski, K. Zagalski, M. Maruszewski, A.L. Jones, L. Cierpka, L.M. de la Fuente, N. L'Heureux, Biomaterials 30 (2009) 1542–1550.
[46] T. Arai, G. Freddi, R. Innocenti, M. Tsukada, J. Appl. Polym. Sci. 91 (2004) 2383–2390.
[47] Y. Wang, D.D. Rudym, A. Walsh, L. Abrahamsen, H.J. Kim, H.S. Kim, C. Kirker-Head, D.L. Kaplan, Biomaterials 29 (2008) 3415–3428.
[48] N. Bhardwaj, S.C. Kundu, Biotechnol. Adv. 28 (2010) 325–347.